

Coherent quantum hairy black holes from gravitational decoupling

Henrique NAVARRO ^{1,*} and Roldao DA ROCHA ^{2,†}

¹*Federal University of ABC, Center of Physics,
Santo André, São Paulo, 09580-210, Brazil*

²*Federal University of ABC, Center of Mathematics,
Santo André, São Paulo, 09580-210, Brazil*

A quantum description of hairy black holes within the gravitational decoupling (GD) is developed using coherent graviton states. Classical geometry emerges as the mean-field limit of a finite graviton condensate, while quantum fluctuations introduce a short-distance regulator. We construct a coherent quantum GD hairy black hole metric by Gaussian-smearing the gravitational potential, with an effective width that encodes the size of the quantum core. The resulting geometry is free of curvature singularities over appropriate parameter ranges and exhibits modified horizon structures. The effective stress–energy tensor is derived, the energy conditions are analyzed, and the Misner–Sharp mass is computed. We investigate geodesics in the coherent quantum GD hairy black hole geometry, with relevant deviations from the RN case. Photon rings, critical impact parameters, and light deflection exhibit measurable strong-field modifications, allowing observational constraints on deviations from general relativity.

I. INTRODUCTION

The detection of gravitational waves (GWs) by laser-interferometric observatories has advanced the understanding of the strong-field regime of gravity [1]. Emitted during the late stages of binary mergers, GWs enable tests of solutions to the Einstein field equations and their extensions. In particular, the ringdown phase of compact binary coalescences is governed by quasinormal modes (QNMs), which are sensitive to deviations from the Kerr and Reissner–Nordström (RN) geometries. Consequently, GW observations provide a powerful probe of black hole hair and short-range modifications of gravity.

The gravitational decoupling (GD) approach has emerged as a robust framework for constructing self-gravitating compact stellar configurations and black holes, from seed solutions in general relativity (GR) [2, 3]. This technique naturally induces anisotropic matter distributions and allows for analytical solutions of the Einstein field equations through the introduction of

*Electronic address: henrique.navarro@ufabc.edu.br

†Electronic address: roldao.rocha@ufabc.edu.br

additional sources in the energy-momentum tensor, encoding tidal and gauge charges, scalar hair, or any contributions from extended theories of gravity [4–11]. Relativistic nuclear theory indicates that stellar interiors at high densities develop pressure anisotropies [12, 13], which are naturally accommodated by the GD method, where the additional gravitational sector induces effective radial and tangential pressures that differ even when starting from isotropic seed solutions [14–21]. The GD approach plays a prominent role in gauge/gravity correspondences, accounting for black hole solutions in the infrared (IR) regime [22–25], including holographic entanglement entropy approaches [26]. GD black holes have been extensively investigated through gravitational lensing analyses [27–29], redshift measurements [30], and studies within analog gravity [31]. An important recent advance is the emergence of black hole solutions with gravitational decoupling (GD) hair [32–38]. These configurations have also been explored in dark matter phenomenology [39–41]. GD hairy black holes possess extra degrees of freedom that are not related to quasilocal conserved charges, and the study of such primary hair contributes meaningfully to the consistent analytical modeling of compact objects and black holes within GR and quantum gravity frameworks. Extensions of GD hairy black holes to asymptotically AdS spacetimes have also been reported [42, 43]. From an observational perspective, their quasinormal mode spectra and associated signatures have been investigated in Refs. [44–50]. The thermodynamic stability of GD hairy black holes has been analyzed in Refs. [51–55], while possible astrophysical accretion scenarios were proposed in Ref. [56].

The nature of spacetime at trans-Planckian scales remains one of the central open problems in gravitational physics. Although classical solutions of GR accurately describe macroscopic phenomena, they generically predict curvature singularities, signaling the breakdown of the theory [57]. Black holes, in particular, suggest that quantum effects must modify the classical description in the high-curvature regime. A relevant framework addressing this issue is provided by the corpuscular, or coherent-state, approach to gravity, in which classical fields emerge as macroscopic quantum states of many weakly interacting quanta [58–60]. The gravitational field can be described as a coherent state of gravitons, and black holes correspond to condensates of¹ $N \sim M^2/M_{\text{p}}^2$ soft gravitons whose collective dynamics reproduce the classical geometry in a mean-field limit [61, 62]. Quantum effects arise from the finite occupation number and manifest themselves as $1/N$ corrections, which become relevant near the would-be singularity or for sufficiently small black holes [63]. This viewpoint is formalized in the quantum N -portrait of black holes [64], which provides a microscopic interpretation of black hole entropy, evaporation, and deviations from exact thermality, predicting the existence of quantum hair [65]. Within

¹ Hereon M_{p} denotes the Planck mass and ℓ_{p} is the Planck scale.

this framework, the coherent state approach to quantum black holes offers a straightforward quantum-mechanical implementation of these ideas, without aiming to constitute an ultraviolet-complete theory of quantum gravity, while capturing leading quantum corrections to the classical black hole geometry. Collective effects of the graviton condensate were further shown to modify semiclassical expectations near the horizon [66]. A thorough quantum field-theoretical approach to graviton bound states is reported in Refs. [67, 68].

Related developments were pursued within effective quantum geometry approaches, where a smeared structure replaces a sharply defined horizon. The horizon properties of quantum black holes were studied in Ref. [69]. They have since been extended to increasingly realistic quantum-corrected Schwarzschild and RN geometries [70], as well as rotating quantum black holes [71, 72]. The role of quantum hair and its contribution to entropy was investigated in Ref. [73], and quantum effects during gravitational collapse were analyzed in Ref. [74]. Black holes with quantum matter cores were proposed in Refs. [75, 76], and the construction of coherent quantum black holes carrying electric charge was accomplished, e.g., in Refs. [77–79]. Therefore, GD hairy black holes can provide a natural arena in which quantum gravitational effects can manifest at horizon scales while remaining consistent with classical behavior at large distances.

An important consequence of the corpuscular or coherent-state picture is the emergence of an intrinsic length scale associated with the spread of the graviton wavefunction. Since a coherent state cannot support arbitrarily short wavelengths, the resulting spacetime geometry is effectively smeared at small scales, providing a natural mechanism for regularizing curvature divergences [80]. Several recent works have implemented this idea by introducing Gaussian or other smearing functions in momentum space, yielding quantum-corrected black hole metrics that are nonsingular and exhibit modified horizon structures [81].

In this work, we construct and analyze coherent quantum GD hairy black holes. Starting from the classical GD hairy black hole metric, we implement quantum corrections through a Gaussian smearing of the gravitational potential, interpreted as a finite-size effect of the underlying graviton condensate. We then extend this procedure to incorporate hairy contributions obtained via GD under dominant energy conditions. The resulting geometry interpolates smoothly between a regular quantum core and the classical asymptotic behavior, while incorporating Yukawa-type and Coulomb-like hair terms. We derive the full coherent quantum GD hairy metric function, compute the effective stress-energy tensor sourcing this spacetime, and analyze the corresponding energy density and pressures. The Misner–Sharp mass is obtained and shown to interpolate between a regular core and a modified asymptotic mass influenced by the hair parameters. We also scrutinize the horizon structure and identify parameter regimes

corresponding to non-extremal, extremal, and horizonless configurations. We also investigate the behavior of curvature invariants near the origin and establish conditions under which the geometry is regular. Our results reinforce the interpretation of black holes as macroscopic quantum objects, whose classical singularities are resolved by finite-graviton-number effects, while emphasizing the nontrivial interplay between quantum corrections and gravitational hair.

This paper is organized as follows. Section II reviews the classical GD hairy black hole, exploring the role of the hair parameter in deforming the RN geometry. Section III introduces the coherent quantum framework with Gaussian regularization, derives the quantum-corrected RN spacetime, and extends it to the GD hairy case, showing that the smearing scale resolves the singularity while preserving large-scale behavior. Section IV is devoted to obtaining the effective stress-energy tensor and the Misner–Sharp mass, delving into quantum effects and the influence of the hairy parameter on the ADM mass. The horizon structure and causal properties are also analyzed. Section V identifies regularity conditions at the origin. Section VI studies geodesics, photon rings, the critical impact parameter, and light deflection, emphasizing deviations from the classical geometry. Finally, Section VII presents conclusions and outlines possible extensions regarding applications of coherent quantum GD hairy black holes.

II. GD HAIRY BLACK HOLES

In this section, the GD framework is briefly reviewed and applied to the construction of GD hairy black hole solutions sourced by an additional gravitational sector [32]. One considers the Einstein field equations²

$$R_{\mu\nu} - \frac{1}{2}Rg_{\mu\nu} = \kappa^2 (T_{\mu\nu} + \theta_{\mu\nu}) , \quad (1)$$

with the total energy-momentum tensor composed by a known seed sector $T_{\mu\nu}$ and an additional source $\theta_{\mu\nu}$ [2, 3]. Since the Einstein tensor obeys the Bianchi identity, the total source must satisfy

$$\nabla^\mu (T_{\mu\nu} + \theta_{\mu\nu}) = 0 . \quad (2)$$

For a static and spherically symmetric geometry,

$$ds^2 = e^{\nu(r)} dt^2 - e^{\lambda(r)} dr^2 - r^2 d\Omega^2 , \quad (3)$$

² We use units with $c = 1$ and $\kappa^2 = 8\pi G_N$, where G_N is the Newton gravitational constant.

the Einstein field equations (1) can be written as (the symbol A' indicates the derivative of a function $A(r)$ with respect to r):

$$\kappa^2(T_0^0 + \theta_0^0) = \frac{1}{r^2} + \frac{e^{-\lambda}}{r} \left(\lambda' - \frac{1}{r} \right), \quad (4a)$$

$$\kappa^2(T_1^1 + \theta_1^1) = \frac{e^{-\lambda}}{r^3} \left(\nu' + \frac{1}{r} \right), \quad (4b)$$

$$\kappa^2(T_2^2 + \theta_2^2) = -\frac{e^{-\lambda}}{4} \left(2\nu'' + \nu'^2 - \lambda'\nu' + 2\frac{\nu' - \lambda'}{r} \right). \quad (4c)$$

The anisotropy term is then defined as $\Pi \equiv p_T - p_R$, with associated effective radial pressure

$$p_R = -T_1^1 - \theta_1^1, \quad (5)$$

effective tangential pressure defined by

$$p_T = -T_2^2 - \theta_2^2, \quad (6)$$

and effective energy density given as

$$\rho = T_0^0 + \theta_0^0, \quad (7)$$

Therefore, for effective sources generated by the GD procedure, a negative effective radial pressure is required when the total energy density is positive. The condition

$$p_R = -\rho \quad (8)$$

is necessary to preserve the existence of a regular Killing horizon and to ensure the GD decoupling. Indeed, the Einstein field equations (4a) – (4c) imply [32]

$$\kappa^2(\rho + p_R) = \frac{e^{-\lambda}}{r} (\nu' + \lambda'). \quad (9)$$

At the horizon $r = r_h$, where $e^{\nu(r_h)} = 0 = e^{-\lambda(r_h)}$, regularity requires Eq. (9) be satisfied only if Eq. (8) holds [32]. Near the horizon, the GD-induced sector behaves like a vacuum-like fluid with equation of state (8), effectively polarizing the gravitational vacuum and generating anisotropic stresses that deform the black hole geometry [32].

In the context of the GD approach, let $\xi(r)$ and $\chi(r)$ compose, respectively, the temporal and radial components of the metric for the seed solution as

$$ds^2 = e^{\xi(r)} dt^2 - e^{\chi(r)} dr^2 - r^2 d\Omega^2, \quad (10)$$

describing the original spacetime geometry before any additional source or deformation is introduced. The standard GR relation

$$e^{-\chi(r)} = 1 - \frac{\kappa^2}{r} \int_0^r dr r^2 T_0^0(r) \equiv 1 - \frac{2m(r)}{r} \quad (11)$$

defines the Misner–Sharp mass $m(r)$, interpolating between the local energy content at finite radius and the total gravitational mass measured at infinity.

Any known seed solution of the Einstein field equations is modified to include the effects of the additional source $\theta_{\mu\nu}$. GD deformations – described in the metric (3) – of the seed metric (10) are introduced to guarantee the separability of the Einstein field equations, as

$$\nu(r) = \xi(r) + \alpha g(r), \quad (12a)$$

$$e^{-\lambda(r)} = e^{-\chi(r)} + \alpha h(r), \quad (12b)$$

where α controls the strength of the GD deformation. Eqs. (12a, 12b) ensure that the Einstein field equations split into two independent systems, one corresponding to the original seed solution and the other associated with the additional gravitational sector. Requiring that the exterior solution remains asymptotically flat and matches the Schwarzschild geometry yields the constraint [32]

$$\alpha h(r) = \left(1 - \frac{2M}{r}\right) \left(e^{\alpha g(r)} - 1\right). \quad (13)$$

In this way, $g(r)$ and $h(r)$ in Eqs. (12a, 12b) introduce the hair generated by the additional source, allowing one to systematically explore deviations from standard GR while maintaining a consistent exterior GD solution. Therefore the line element (3) yields

$$ds^2 = \left(1 - \frac{2M}{r}\right) e^{\alpha g(r)} dt^2 - \left(1 - \frac{2M}{r}\right)^{-1} e^{-\alpha g(r)} dr^2 - r^2 d\Omega^2. \quad (14)$$

Besides, the seed energy-momentum tensor is conserved with respect to the seed metric components in (10):

$$\nabla_{\mu}^{(\xi, \chi)} (T^{\mu}_{\nu} + \theta^{\mu}_{\nu}) = 0. \quad (15)$$

Substituting the GD deformations (12a, 12b) into the Einstein field equations yields two independent systems. The first one comprises the seed sector, represented by

$$\kappa^2 T_0^0 = \frac{1}{r^2} - \frac{e^{-\chi}}{r} \left(\frac{1}{r} - \chi'\right), \quad (16a)$$

$$\kappa^2 T_1^1 = \frac{1}{r^2} - \frac{e^{-\chi}}{r} \left(\frac{1}{r} + \xi'\right), \quad (16b)$$

$$\kappa^2 T_2^2 = -\frac{e^{-\chi}}{4} \left(2\xi'' + \xi'^2 - \chi'\xi' + 2\frac{\xi' - \chi'}{r}\right). \quad (16c)$$

The second sector consists of the quasi-Einstein system for the additional source $\theta_{\mu\nu}$ [32, 82, 83]:

$$\kappa^2 \theta_0^0 = -\frac{\alpha}{r} \left(\frac{h}{r} + h' \right), \quad (17a)$$

$$\kappa^2 \theta_1^1 + \alpha \mathfrak{z}_1 = -\frac{\alpha h}{r} \left(\frac{1}{r} + \nu' \right), \quad (17b)$$

$$\kappa^2 \theta_2^2 + \alpha \mathfrak{z}_2 = -\frac{\alpha h}{4} \left(2\nu'' + \nu'^2 + 2\frac{\nu'}{r} \right) - \frac{\alpha h'}{4} \left(\nu' + \frac{2}{r} \right), \quad (17c)$$

with

$$\mathfrak{z}_1 = \frac{e^{-\chi} g'}{r}, \quad (18a)$$

$$\mathfrak{z}_2 = \frac{e^{-\chi}}{4} \left(2g'' + g'^2 + \frac{2g'}{r} + 2\xi' g' - \chi' g' \right). \quad (18b)$$

Clearly $\lim_{\alpha \rightarrow 0} \theta_{\mu\nu} = 0$, and for $g = 0$ the quasi-Einstein system (17a) – (17c) reduces to the minimal geometric deformation in Ref. [2].

The conservation equation (2) becomes

$$\nabla_\sigma T^\sigma{}_\nu = \nabla_\sigma^{(\xi, \chi)} T^\sigma{}_\nu - \alpha \frac{g'}{2} (T_0^0 - T_1^1) \delta_\nu^1, \quad (19)$$

where the first term on the right-hand side of (19) vanishes due to the conservation law in Eq. (15). Using the full metric (3), the total conservation law then gives

$$0 = \nabla_\sigma T^\sigma{}_\nu + \nabla_\sigma \theta^\sigma{}_\nu = (\theta_1^1)' - \frac{\nu'}{2} (\theta_0^0 - \theta_1^1) - \frac{2}{r} (\theta_2^2 - \theta_1^1) - \alpha \frac{g'}{2} (T_0^0 - T_1^1), \quad (20)$$

which is a linear combination of Eqs. (17a) – (17c). Thus the seed sector $T_{\mu\nu}$ and the additional source $\theta_{\mu\nu}$ are fully decoupled by the GD. This protocol was extended in the context of Lovelock gravity [84], Brans-Dicke gravity [85], Riemann–Cartan spacetimes, and Einstein–Maxwell-scalar gravities [86–89].

The dominant energy condition (DEC) requires

$$\rho \geq |p_R|, \quad (21a)$$

$$\rho \geq |p_T|. \quad (21b)$$

Using Eq. (8) yields the only nontrivial condition (21b) which, using Eqs. (6, 7), is equivalent to [32] the two inequalities:

$$\theta_0^0 + \theta_2^2 \geq 0, \quad \theta_0^0 - \theta_2^2 \geq 0. \quad (22)$$

Defining the radial function

$$k(r) \equiv e^{\alpha g(r)}, \quad (23)$$

and using Eqs. (17a) and (17c), the first inequality in (22) yields

$$\mathcal{H}_1(r) \equiv r(r - 2G_N M)k''(r) + 4(r - G_N M)k'(r) + 2k(r) - 2 \leq 0, \quad (24)$$

One looks for deformations that satisfy the inequality (24) near the horizon $r \approx 2G_N M$ and at the outer geometry $r \gg M$.

The differential inequality (24) admits a family of admissible deformations compatible with the DEC. To proceed analytically, one focuses on solutions that saturate the inequality (24), with a source [32]

$$\mathcal{H}_1(r) = \frac{\alpha}{G_N M}(r - 2G_N M)e^{-r/(G_N M)}. \quad (25)$$

Therefore, the solution of the resulting equation is given by

$$k(r) = 1 - \frac{1}{r - 2G_N M} \left[\alpha \ell + \alpha G_N M e^{-r/(G_N M)} - \frac{G_N Q^2}{r} \right], \quad (26)$$

where ℓ and Q encode the black hole hair proportional to α . Substituting the function (26) into the metric (14), using Eq. (23), finally yields the GD hairy black hole metric coefficients of the metric (3), with Yukawa-type exponential term [32]:

$$e^{\nu(r)} = e^{-\lambda(r)} = 1 - \frac{2G_N M + \alpha G_N \ell}{r} + \frac{G_N Q^2}{r^2} - \frac{\alpha G_N M}{r} e^{-r/(G_N M)}, \quad (27)$$

An important aspect of the GD hairy black hole solution under DEC is that it does not allow for arbitrary values of the hair charges ℓ and Q , since it requires a horizon radius $r_h \geq 2G_N M$. Ref. [32] shows that these charges must present the following lower bounds:

$$Q^2 \geq \frac{4\alpha M^2}{e^2}, \quad \ell \geq \frac{M}{e^2}. \quad (28)$$

III. COHERENT QUANTUM GD HAIRY BLACK HOLES

For static, spherically symmetric and asymptotically flat configurations, the line element can be written as

$$ds^2 = -f(r) dt^2 + \frac{dr^2}{f(r)} + r^2 d\Omega^2, \quad (29)$$

with

$$f(r) \equiv 1 + 2V(r), \quad (30)$$

where r denotes the areal radius, and the horizons are determined by the solutions of $f(r) = 0$. We will show that the GD hairy solution (3, 27) represents a classical spacetime geometry that

can be interpreted as the expectation value of a coherent quantum GD hairy metric operator evaluated on a suitable coherent state built upon the Minkowski vacuum [58, 63]. This approach allows one to encode the gravitational field in an effective potential that appears in the metric. A static and spherically symmetric gravitational potential $V(r)$ can be identified with the expectation value of a canonically normalized free massless scalar field operator Φ evaluated over a coherent state $|g\rangle$ [59],

$$\langle g | \Phi(t, r) | g \rangle = V(r). \quad (31)$$

The scalar field Φ does not represent a fundamental matter degree of freedom, but provides an effective description of the collective, non-perturbative quantum degrees of freedom underlying the classical geometry. The quantization of the scalar field can be implemented by first rescaling the dimensionless potential V as

$$V(r) \mapsto \sqrt{\frac{m_{\text{P}}}{\ell_{\text{P}}}} V(r), \quad (32)$$

so that Φ satisfies the free massless Klein–Gordon equation,

$$(-\partial_t^2 + \nabla^2) \Phi(t, r) = 0, \quad (33)$$

whose complete set of solutions is given by $\mathbf{u}_k(t, r) = e^{-ikt} j_0(kr)$, where $j_0(kr) = \frac{\sin(kr)}{kr}$ is the zeroth order spherical Bessel function, with $k > 0$. The field operator and its conjugate momentum, respectively, read

$$\Phi(t, r) = \frac{1}{2\pi^2} \int_0^\infty k^2 dk \sqrt{\frac{\hbar}{2k}} \left[a_k \mathbf{u}_k(t, r) + a_k^\dagger \mathbf{u}_k^*(t, r) \right], \quad (34a)$$

$$\Pi(t, r) = \frac{i}{2\pi^2} \int_0^\infty k^2 dk \sqrt{\frac{\hbar k}{2}} \left[a_k \mathbf{u}_k(t, r) - a_k^\dagger \mathbf{u}_k^*(t, r) \right], \quad (34b)$$

where the creation and annihilation operators satisfy $[a_k, a_p^\dagger] = \frac{2\pi^2}{k^2} \delta(k - p)$. Classical field configurations are reproduced by coherent states $|g\rangle$ defined as eigenstates of the annihilation operators,

$$a_k |g\rangle = g_k e^{ikt} |g\rangle, \quad (35)$$

removing explicit time dependence on the expectation value, for static potentials. Writing the Fourier–Bessel decomposition

$$V(r) = \frac{1}{2\pi^2} \int_0^\infty k^2 \tilde{V}(k) j_0(kr) dk, \quad (36)$$

one finds in Eq. (35)

$$g_k = \sqrt{\frac{k}{2}} \frac{\tilde{V}(k)}{\ell_{\text{P}}}. \quad (37)$$

The coherent state then reads

$$|g\rangle = \frac{e^{-N_G/2}}{2\pi^2} \exp\left[\int_0^\infty k^2 g_k dk a_k^\dagger\right] |0\rangle, \quad (38)$$

with the total occupation number

$$N_G = \frac{1}{2\pi^2} \int_0^\infty k^2 g_k^2 dk. \quad (39)$$

When applied to the RN geometry with $\alpha = 0$ in the metric (3, 27), the classical potential cannot be exactly reproduced by a normalizable coherent state due to ultraviolet (UV) divergences associated with high-momentum modes [70]. This obstruction is resolved by introducing a finite smearing scale R_s , interpreted as the size of the quantum core, and implementing a Gaussian regulator. The resulting quantum-corrected GD hairy potential remains asymptotically RN at large distances while yielding a regular geometry at short scales, providing a consistent effective description of charged black holes within the coherent-state formalism [78].

The scalar field Φ in Eq. (34a) effectively describes the quantum constituents that make classical geometry to emerge. For the RN geometry, the classical gravitational potential reads

$$V_{\text{RN}}(r) = -\frac{G_N M}{r} + \frac{G_N Q^2}{2r^2}, \quad (40)$$

where M and Q denote the ADM mass and electric charge. Within the coherent-state setup, the potential (40) cannot be exactly reproduced by a normalizable coherent state of a free massless scalar field due to UV divergences in the occupation number from arbitrarily large-momentum modes [58, 63]. In particular, the r^{-2} term yields a slow decay of the Fourier–Bessel transform at large k , making the total occupation number divergent and the coherent state non-normalizable [70].

To cure this issue, one introduces a finite smearing scale R_s , interpreted as the characteristic size of the quantum core, and adopts a Gaussian regulator rather than a sharp UV cutoff to avoid spurious oscillations in position space. This smoothly suppresses high-momentum modes while preserving the large-distance behavior of the classical solution. For a spherically symmetric configuration, the Gaussian-regularized quantum expectation value of the potential reads

$$V_{\text{RN}}^q(r) = \frac{1}{2\pi^2} \int_0^\infty k^2 \tilde{V}_{\text{RN}}(k) e^{-k^2 R_s^2/4} j_0(kr) dk, \quad (41)$$

where the Fourier–Bessel transform of the classical RN potential (40) is given by

$$\tilde{V}_{\text{RN}}(k) = -\frac{4\pi G_N M}{k^2} + \frac{\pi^2 G_N Q^2}{k}. \quad (42)$$

The Gaussian factor $e^{-k^2 R_s^2/4}$ in Eq. (41) suppresses large-momentum modes, implementing a minimal-length smearing of width R_s in position space. Physically, this replaces point-like mass

and charge distributions with Gaussian profiles, removing the UV modes responsible for the classical curvature singularity.

Computing the integral (41) yields

$$V_{\text{RN}}^q(r) = -\frac{G_{\text{N}}M}{r} \operatorname{erf}\left(\frac{r}{R_{\text{s}}}\right) + \frac{G_{\text{N}}Q^2}{r R_{\text{s}}} \operatorname{F}\left(\frac{r}{R_{\text{s}}}\right), \quad (43)$$

where $\operatorname{erf}(x)$ is the error function and $\operatorname{F}(x) = e^{-x^2} \int_0^x e^{t^2} dt$ is the Dawson function. The Gaussian smearing modifies only the short-distance sector while leaving the IR behavior intact. For $r \gg R_{\text{s}}$, the classical RN potential can be recovered. On the other hand, near the origin, one can expand Eq. (43), yielding

$$V_{\text{RN}}^q(r) = -\frac{2G_{\text{N}}M}{\sqrt{\pi}R_{\text{s}}} + \frac{G_{\text{N}}Q^2}{R_{\text{s}}^2} + \mathcal{O}(r^2). \quad (44)$$

The singular r^{-1} and r^{-2} behaviors are therefore replaced by a finite constant core, implying that the effective gravitational field vanishes linearly as $r \rightarrow 0$. The central RN geometry is thus regular, with curvature invariants remaining finite, and the classical RN singularity is resolved by the Gaussian smearing [78]. Introducing the definitions

$$R_{\text{M}} \equiv 2G_{\text{N}}M, \quad R_{\text{Q}} \equiv \sqrt{G_{\text{N}}}Q, \quad (45)$$

the quantum-corrected RN metric function becomes [78]

$$f(r) = 1 - \frac{R_{\text{M}}}{r} \operatorname{erf}\left(\frac{r}{R_{\text{s}}}\right) + \frac{2R_{\text{Q}}^2}{r R_{\text{s}}} \operatorname{F}\left(\frac{r}{R_{\text{s}}}\right). \quad (46)$$

Expanding around the origin, one finds

$$f(r) = 1 - \frac{2R_{\text{M}}}{\sqrt{\pi}R_{\text{s}}} + \frac{2R_{\text{Q}}^2}{R_{\text{s}}^2} + \mathcal{O}(r^2), \quad (47)$$

so that $\lim_{r \rightarrow 0} f(r)$ is finite and the quantum RN spacetime is regular at the origin. The Gaussian width R_{s} acts moreover as a fundamental scale controlling the transition between a classical exterior geometry and a nonsingular quantum core.

Now let us consider the GD hairy black hole solution (27), whose potential can be split as the sum of an RN part and a hairy component, as

$$V(r) = V_{\text{RN}}(r) + V_{\text{H}}(r), \quad (48)$$

with

$$V_{\text{H}}(r) = \frac{\alpha G_{\text{N}}}{2r} \left(M e^{-r/(G_{\text{N}}M)} - \ell \right). \quad (49)$$

The exponential term introduces a Yukawa-type correction characterized by the scale $G_{\text{N}}M$, while the parameter ℓ renormalizes the effective mass, as given in the classical GD hairy metric

(27). Classically, these terms alter the near-horizon structure, but retain the short-distance divergence.

Applying Gaussian regularization to the quantum hairy part of the potential yields

$$V_H^q(r) = \frac{\alpha G_N M}{2r} e^{R_s^2/(2G_N M)^2} \left[e^{-r/(G_N M)} \operatorname{erfc}\left(\frac{R_s}{2G_N M} - \frac{r}{R_s}\right) - e^{r/(G_N M)} \operatorname{erfc}\left(\frac{R_s}{2G_N M} + \frac{r}{R_s}\right) \right] + \frac{\alpha G_N \ell}{2r} \operatorname{erf}\left(\frac{r}{R_s}\right), \quad (50)$$

which remains finite as $r \rightarrow 0$, ensuring that the additional GD hair does not reintroduce a curvature singularity. The complete quantum-corrected GD hairy potential can be expressed as

$$V_{\text{GDH}}^q(r) = V_{\text{RN}}^q(r) + V_H^q(r), \quad (51)$$

and the metric function (27) takes the form

$$f(r) = 1 + 2V_{\text{GDH}}^q(r). \quad (52)$$

For $\alpha \rightarrow 0$, the quantum RN geometry can be recovered. For a nonvanishing hairy parameter α , the regular quantum core persists. The Gaussian smearing simultaneously resolves the central singularity and regularizes the additional hair contributions, without modifying the asymptotic RN behavior.

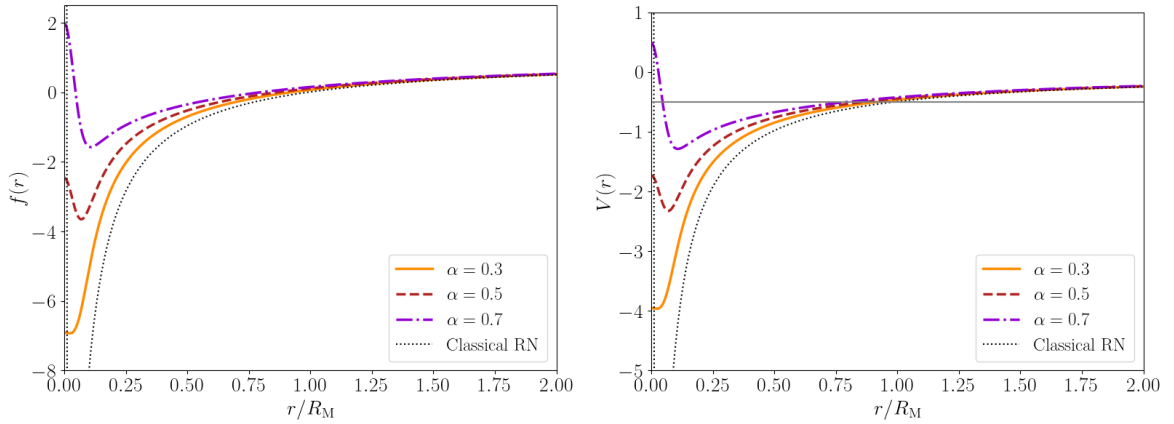


FIG. 1: Metric function (left) and potential function (right) for the coherent quantum GD hairy black hole, with $R_s/R_M = 0.05$ and $R_Q/R_M = 0.1$.

Figs. 1 and 2 present the radial profile of the coherent quantum GD metric function $f(r)$ and their corresponding potential $V_{\text{GDH}}^q(r)$ for different values of the hairy parameter α and representative choices of R_s/R_M and R_Q/R_M . As α increases, the magnitude of $f(r)$ in the inner region is enhanced, particularly for larger R_Q/R_M , while the qualitative decay pattern at small r/R_M is preserved. In all cases, the solutions converge to a common asymptotic behavior

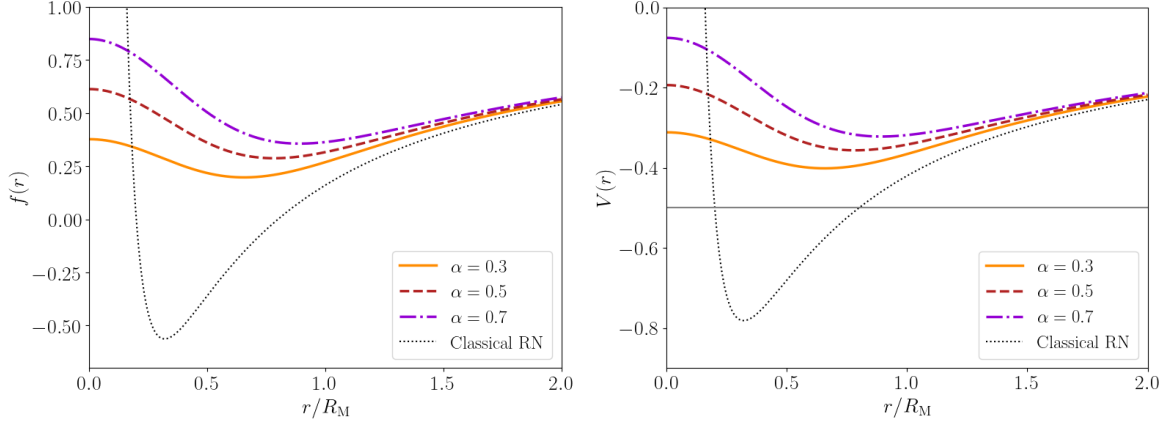


FIG. 2: Metric function (left) and potential function (right) for the coherent quantum GD hairy black hole, with $R_s/R_M = 0.5$ and $R_Q/R_M = 0.4$.

at large radii, indicating that variations in α , R_s , and R_Q predominantly affect the near-core structure of the geometry.

A more illustrative view of our results is depicted in Fig. 3, for some values of R_s/R_M and R_Q/R_M . Fig. 3 shows the two-dimensional profile of the the coherent quantum GD hairy metric function $f(r, \alpha)$ as a function of the radial coordinate and the hairy parameter, for different choices of the ratios R_s/R_M and R_Q/R_M . For parameter sets with larger R_Q/R_M , the coherent quantum GD hairy metric function $f(r, \alpha)$ exhibits a steep increment near the inner region, followed by a rapid suppression and a smooth approach to its asymptotic regime. On the other hand, configurations with smaller R_Q/R_M display a milder radial dependence and a smoother evolution in terms of the hairy parameter α , indicating that the combined effect of R_s and R_Q primarily controls the near-core structure of the coherent quantum GD hairy solution.

For completeness, let us regard the coherent quantum GD hairy metric (29), whose components (52) are associated with the potential (51) as

$$V_{\text{GDH}}^q(r) = -\frac{R_M}{2r} \operatorname{erf}\left(\frac{r}{R_s}\right) + \frac{R_Q^2}{rR_s} F\left(\frac{r}{R_s}\right) + \frac{\alpha G_N \ell}{2r} \operatorname{erf}\left(\frac{r}{R_s}\right) + \frac{\alpha}{4r} R_M e^{R_s^2/R_M^2} \left[e^{-2r/R_M} \operatorname{erfc}\left(\frac{R_s}{R_M} - \frac{r}{R_s}\right) - e^{2r/R_M} \operatorname{erfc}\left(\frac{R_s}{R_M} + \frac{r}{R_s}\right) \right]. \quad (53)$$

Since the event horizon \hat{r} is determined by the equation $f(\hat{r}) = 0$, the coherent quantum GD hairy black hole metric (52) makes it correspond to

$$V_{\text{GDH}}^q(\hat{r}_{\pm}) = -\frac{1}{2}, \quad (54)$$

whose solutions are not algebraic. Nevertheless, the qualitative structure of horizons can be inferred from the behavior of the potential. First, $\lim_{r \rightarrow \infty} \operatorname{erf}(r/R_s) = 1$ and the exponentially

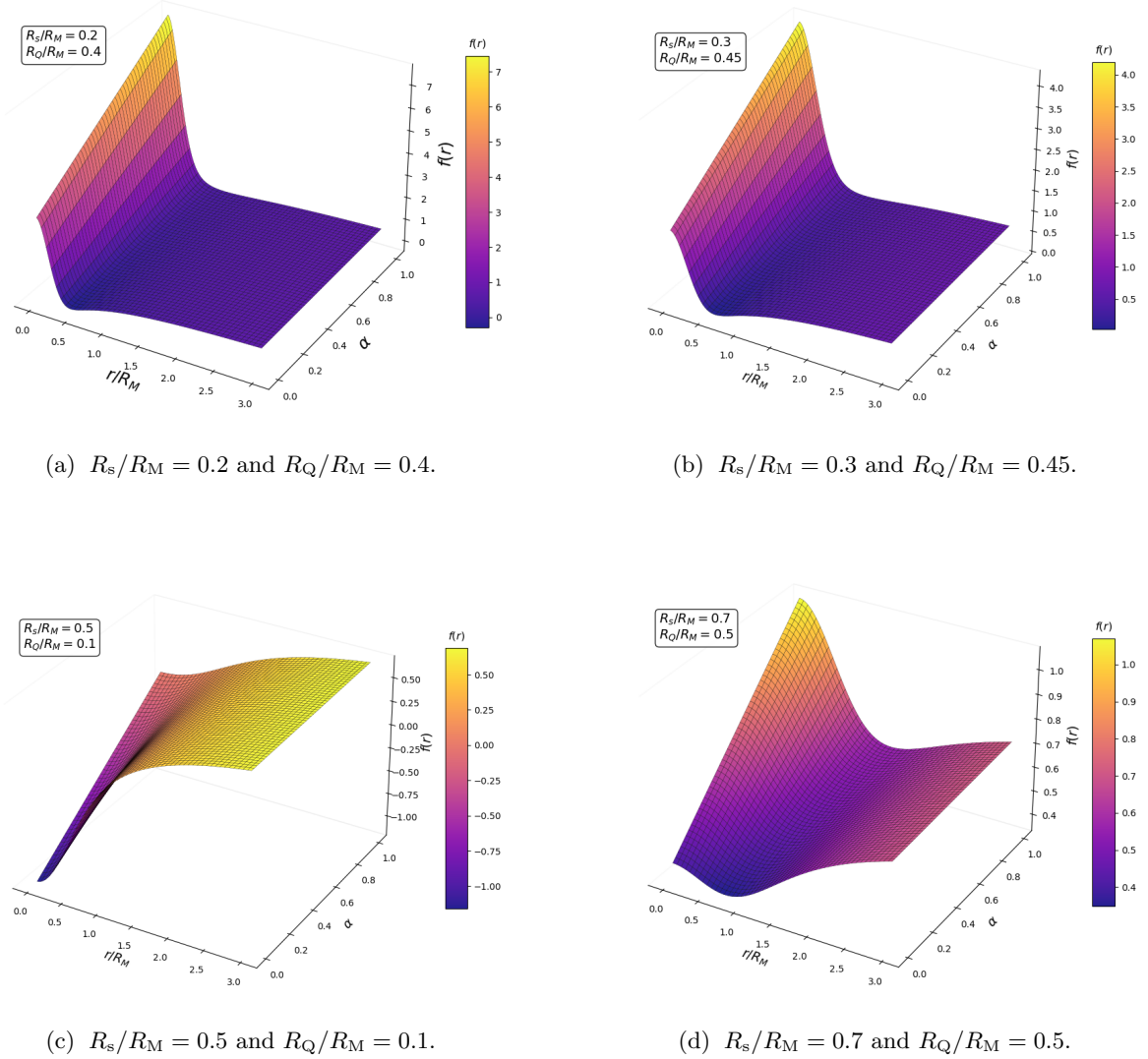


FIG. 3: Metric function $f(r, \alpha)$ for different values of the ratios R_s/R_M and R_Q/R_M .

suppressed erfc terms vanish in this limit, yielding

$$\lim_{r \rightarrow \infty} V_{\text{GDH}}^q(r) = 0. \quad (55)$$

Hence, the coherent quantum GD hairy spacetime remains asymptotically flat. Depending on the combination of parameters (R_M, R_Q, R_s, α) , three scenarios arise. The first one comprises two distinct horizons (non-extremal), the second possibility regards a degenerate horizon (extremal or multiplicity-two solution), and the third case lacks an event horizon, in which case the singularity is naked in the classical sense, although resolved in the quantum-mechanical setup.

Near the origin, the Gaussian regularization and the quantum hair smooth the classical singularity, with

$$\lim_{r \rightarrow 0^+} V_{\text{GDH}}^q(r) = \frac{R_Q^2}{R_s^2} - \frac{R_M}{\sqrt{\pi} R_s} \left[1 - \alpha \left(1 + \frac{G_N \ell}{R_M} \right) \right] - \alpha e^{R_s^2/R_M^2} \operatorname{erfc} \left(\frac{R_s}{R_M} \right). \quad (56)$$

Physically, this limit quantifies the strength of the quantum core and the hair near the origin. The classical r^{-1} divergence is replaced by a finite value determined by R_s and α , reflecting the resolution of the central singularity. If this central value reaches $-1/2$, a horizon emerges at or near the core. Otherwise, the quantum GD hairy geometry may be horizonless, representing a compact quantum object where the would-be singularity is softened. The competition between the mass, charge, quantum core size, and hair amplitude α thus dictates the causal structure of the coherent quantum GD hairy spacetime, specifying how quantum effects and the additional GD source alter horizon formation and the inner geometry relative to classical RN black holes.

IV. EFFECTIVE SOURCE IN THE COHERENT QUANTUM GD HAIRY SOLUTION

The quantum-corrected GD hairy black hole metric (52) can be written as

$$f(r) = f^q(r) + f^H(r), \quad (57)$$

where

$$f^q(r) = 1 - \frac{R_M}{r} \operatorname{erf}\left(\frac{r}{R_s}\right) + \frac{R_Q^2}{r^2} \frac{2r}{R_s} F\left(\frac{r}{R_s}\right), \quad (58)$$

represents the Gaussian-regularized quantum correction to the RN geometry [78], while the GD hairy contribution reads

$$f^H(r) = \frac{\alpha R_M e^{R_s^2/R_M^2}}{2r} \left[e^{-2r/R_M} \operatorname{erfc}\left(\frac{R_s}{R_M} - \frac{r}{R_s}\right) - e^{2r/R_M} \operatorname{erfc}\left(\frac{R_s}{R_M} + \frac{r}{R_s}\right) \right] + \frac{\alpha G_N \ell}{r} \operatorname{erf}\left(\frac{r}{R_s}\right). \quad (59)$$

The coherent quantum GD hairy metric function (57) does not correspond to any known vacuum solution of the Einstein field equations. Nevertheless, the presence of the quantum core scale R_s suggests that the coherent quantum GD hairy geometry is sourced by an effective matter distribution describing a quantum-corrected extended object rather than a point singularity. It is therefore natural to reconstruct the stress-energy tensor directly from the Einstein field equations,

$$T_\nu^\mu = \frac{1}{8\pi G_N} \left(R_\nu^\mu - \frac{1}{2} R g_\nu^\mu \right) = \operatorname{diag}(-\rho, p_r, p_t, p_t), \quad (60)$$

in terms of the energy density, the radial pressure, and the tangential pressure associated with the coherent quantum GD hairy black hole metric (57). Using the lower bound condition over

the hairy parameter $\ell = M/e^2$, defined in Eq. (28), these quantities read

$$\begin{aligned}\rho(r) = -p_r(r) &= \frac{1 - f(r) - rf'(r)}{8\pi G_N r^2} \\ &= \rho_M \frac{R_s^2}{r^2} e^{-r^2/R_s^2} \left[1 - \alpha \left(1 + \frac{1}{2e^2} \right) \right] - 2\rho_Q(r) \frac{r^2}{R_s^2} \left(1 - \frac{2r}{R_s} F\left(\frac{r}{R_s}\right) \right) \\ &\quad + \frac{\alpha e^{R_s^2/R_M^2}}{8\pi G_N r^2} \left[e^{2r/R_M} \operatorname{erfc}\left(\frac{R_s}{R_M} + \frac{r}{R_s}\right) + e^{-2r/R_M} \operatorname{erfc}\left(\frac{R_s}{R_M} - \frac{r}{R_s}\right) \right],\end{aligned}\quad (61)$$

where

$$\rho_M \equiv \frac{M}{2\pi^{3/2} R_s^3}, \quad \rho_Q(r) \equiv \frac{Q^2}{8\pi r^4}.\quad (62)$$

The relation $\rho = -p_r$ indicates a vacuum-like equation of state in the radial direction near the center. The first term on the right-hand side of Eq. (61) corresponds to a Gaussian mass distribution of width R_s , the second one reproduces the regularized electromagnetic contribution, and the remaining terms encode the nontrivial hairy corrections. The Gaussian factor ensures that the mass density is exponentially suppressed at large distances and finite at the origin, while the charge contribution is softened relative to the classical r^{-4} behavior due to the Dawson function term. The hairy parameter α controls the strength of deviations from the pure coherent quantum RN core.

Besides, the tangential pressure takes the form

$$\begin{aligned}p_t(r) &= \frac{2f'(r) + rf''(r)}{16\pi G_N r} \\ &= \rho_M e^{-r^2/R_s^2} \left[1 - \alpha \left(1 + \frac{1}{2e^2} \right) \right] - 2\rho_Q(r) \frac{r^5}{R_s^5} \left[\frac{R_s}{r} - \left(2 - \frac{R_s^2}{r^2} \right) F\left(\frac{r}{R_s}\right) \right] \\ &\quad - \frac{\alpha e^{R_s^2/R_M^2}}{16\pi G_N R_M r} \left[e^{2r/R_M} \operatorname{erfc}\left(\frac{R_s}{R_M} + \frac{r}{R_s}\right) - e^{-2r/R_M} \operatorname{erfc}\left(\frac{R_s}{R_M} - \frac{r}{R_s}\right) \right].\end{aligned}\quad (63)$$

Conversely to the classical RN case, all components of the effective stress-energy tensor (60) remain finite as $r \rightarrow 0$. In particular, the tangential pressure (63) approaches a constant value at the origin, evincing the presence of a regular anisotropic fluid core rather than a curvature singularity. The difference between p_r and p_t in Eqs. (61) and (63) encodes the intrinsic anisotropy induced by the combined quantum smearing and hair contributions. The quantum-corrected GD hairy solution may therefore be interpreted as sourced by a self-gravitating anisotropic quantum fluid whose characteristic length scale is set by R_s and whose deviations from the quantum RN case are governed by the hairy parameter α .

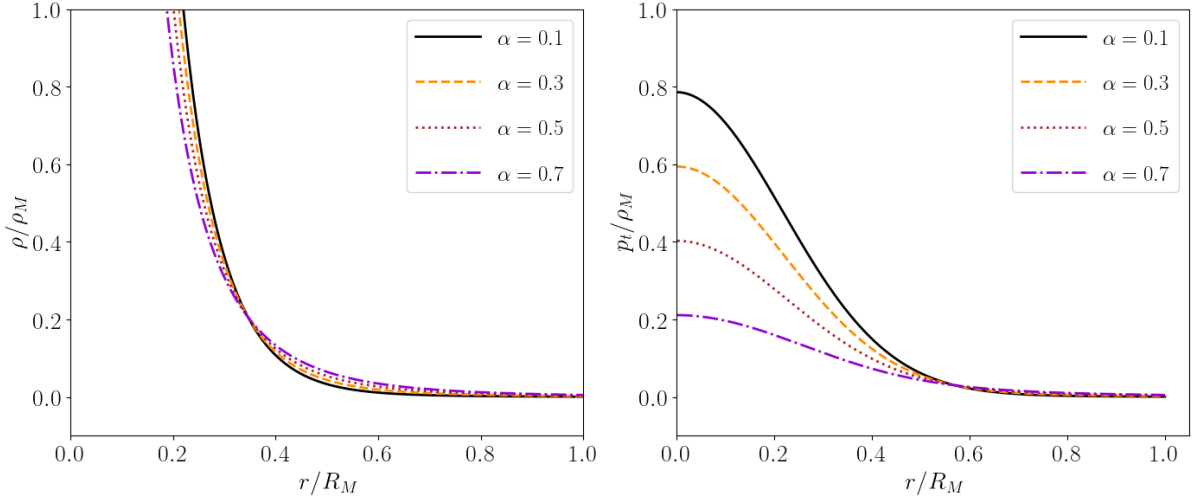


FIG. 4: Normalized effective energy density (left) and normalized tangential pressure (right) for $R_s/R_M = 0.3$, $R_Q/R_M = 0.1$ and $\ell = M/e^2$.

Fig. 4 displays the normalized effective energy density ρ/ρ_M (left panel) and the normalized tangential pressure p_t/ρ_M (right panel) as functions of r/R_M for different values of the hairy parameter α . As α increases, both quantities are suppressed in the inner region, while their radial profiles remain monotonic and rapidly decay toward zero at large radii. This behavior indicates that increasing α weakens the effective matter content near the quantum core of the coherent quantum GD hairy distribution, without altering the asymptotic structure of the configuration.

We can now scrutinize the behavior of the total energy density and tangential pressure in Eqs. (61) and (63), respectively, for two important regimes. The first one regards $r/R_s \gg 1$, corresponding to a large distance from the quantum core, whereas the second relevant regime consists of $r \rightarrow 0^+$, as close as possible to the center. For the coherent quantum GD hairy black hole, the quantum part of both the energy density and tangential pressure functions, $\rho^q(r)$ and $p_t^q(r)$, respectively, are known to asymptotically approach $\rho_Q(r)$ for $r/R_s \gg 1$, emulating the results obtained for the quantum RN part for the whole coherent quantum GD hairy black hole [78]. In addition, since the Dawson function can be expanded as

$$\lim_{r/R_s \gg 1} F\left(\frac{r}{R_s}\right) = \frac{R_s}{2r} + \frac{R_s^3}{4r^3} + \dots \quad (64)$$

the quantum energy density can be reduced to

$$\rho^q(r) \approx 2\rho_Q(r) \frac{r^2}{R_s^2} \left[1 - 2\frac{r}{R_s} \left(\frac{R_s}{2r} + \frac{R_s^3}{4r^3} \right) \right] = \rho_Q(r), \quad (65)$$

and using the fact that the complementary error function has the following asymptotic behavior $\lim_{x \rightarrow \infty} \operatorname{erfc}(x) = 0$, whereas $\lim_{x \rightarrow -\infty} \operatorname{erfc}(x) = 2$, the total energy density in the limit of $r/R_s \gg 1$

becomes

$$\rho(r) = \rho_Q(r) + \frac{\alpha e^{R_s^2/R_M^2}}{4\pi G_N} \frac{e^{-2r/R_M}}{r^2}. \quad (66)$$

Similarly, the total tangential pressure at large distances from the quantum core is given by

$$p_t(r) = \rho_Q(r) + \frac{\alpha e^{R_s^2/R_M^2}}{4\pi G_N R_M} \frac{e^{-2r/R_M}}{2r}. \quad (67)$$

Eq. (66) shows that the energy density decays exponentially and with a r^{-2} rate, while still carrying the hair charge α effects for long distances. The tangential pressure in Eq. (67) presents a Yukawa-like decaying behavior, while also carrying the hair charge α along.

In the limit for $r \rightarrow 0^+$, the quantum energy density and tangential pressure terms have been shown to be reduced to [78]

$$\rho^q(r) = -p_r^q(r) = [\rho_M - 2\rho_Q(R_s)] \frac{R_s^2}{r^2} + \mathcal{O}(1), \quad (68)$$

$$p_t^q(r) = \rho_M - 4\rho_Q(R_s) + \mathcal{O}(r^2). \quad (69)$$

The expansion of the hairy term of the total energy density (61) around $r = 0$ yields

$$\lim_{r \rightarrow 0^+} \rho^H(r) = \left[\frac{e^{R_s^2/R_M^2}}{4\pi G_N R_s^2} \operatorname{erfc}\left(\frac{R_s}{R_M}\right) - \rho_M \left(1 + \frac{1}{2e^2}\right) \right] \alpha \frac{R_s^2}{r^2} + \mathcal{O}(1). \quad (70)$$

The total energy density when $r \rightarrow 0^+$ corresponds to the combination of Eqs. (68) and (70), so that it becomes

$$\rho(r) = \left[\rho_M \left(1 - \alpha \left(1 + \frac{1}{2e^2}\right)\right) - 2\rho_Q(R_s) + \frac{\alpha e^{R_s^2/R_M^2}}{4\pi G_N R_s^2} \operatorname{erfc}\left(\frac{R_s}{R_M}\right) \right] \frac{R_s^2}{r^2}. \quad (71)$$

Similarly, the expansion of the hairy term of the tangential pressure is given by

$$\lim_{r \rightarrow 0^+} p_t^H(r) = -2\alpha\rho_M\sqrt{\pi} \frac{R_s^3}{R_M^3} \operatorname{erfc}\left(\frac{R_s}{R_M}\right) e^{R_s^2/R_M^2} - \alpha\rho_M \left(1 + \frac{1}{2e^2}\right) + 2\alpha\rho_M \frac{R_s^2}{R_M^2} + \mathcal{O}(r^2). \quad (72)$$

Grouping it with the quantum part, the total tangential pressure can be written, up to $\mathcal{O}(r^2)$, as

$$\lim_{r \rightarrow 0^+} p_t(r) = \rho_M - 2\alpha\rho_M \left[\frac{1}{2} \left(1 + \frac{1}{2e^2}\right) + \frac{R_s^3}{R_M^3} \left(\sqrt{\pi} \operatorname{erfc}\left(\frac{R_s}{R_M}\right) e^{R_s^2/R_M^2} - \frac{R_M}{R_s} \right) \right] - 4\rho_Q(R_s). \quad (73)$$

Eq. (71) shows that the energy density and radial pressure diverge at $r = 0$, unless the coefficients cancel r^{-2} . Meanwhile, the tangential pressure remains finite, due to Eq. (73), which can also be realized in Fig. 4.

From the total energy density (61), it is possible to compute the Misner–Sharp mass for the quantum hairy geometry, reading

$$m(r) = 4\pi \int_0^r \rho(r) r^2 dr. \quad (74)$$

Integration performed over the quantum energy density $\rho^q(x)$ yields the result found in Ref. [78], which can be written as

$$m^q(r) = M \operatorname{erf} \left(\frac{r}{R_s} \right) - \frac{Q^2}{R_s} F \left(\frac{r}{R_s} \right). \quad (75)$$

Integration over the hairy energy density $\rho^H(r)$ yields the hairy contribution to the total Misner–Sharp mass, which can be read as

$$m^H(r) = \frac{\alpha}{2} M e^{R_s^2/R_M^2} \left[e^{2r/R_M} \operatorname{erfc} \left(\frac{r}{R_s} + \frac{R_s}{R_M} \right) + e^{-2r/R_M} \operatorname{erfc} \left(\frac{r}{R_s} - \frac{R_s}{R_M} \right) - 2e^{-2r/R_M} \right] - \frac{\alpha M}{2e^2} \operatorname{erf} \left(\frac{r}{R_s} \right), \quad (76)$$

where we used the lower bound over the hairy parameter $\ell = M/e^2$ (28).

The Misner–Sharp mass for the quantum-corrected GD hairy solution can be written as

$$m(r) = M \operatorname{erf} \left(\frac{r}{R_s} \right) \left(1 - \frac{\alpha}{2e^2} \right) - \frac{Q^2}{R_s} F \left(\frac{r}{R_s} \right) + \frac{\alpha}{2} M e^{R_s^2/R_M^2} \left[e^{2r/R_M} \operatorname{erfc} \left(\frac{r}{R_s} + \frac{R_s}{R_M} \right) + e^{-2r/R_M} \operatorname{erfc} \left(\frac{r}{R_s} - \frac{R_s}{R_M} \right) - 2e^{-2r/R_M} \right]. \quad (77)$$

For large values of r , the quantum corrected part $m^q(r)$ yields the ADM mass of the system [78], namely

$$\lim_{r \rightarrow +\infty} m^q(r) = M. \quad (78)$$

However, the hairy correction terms do not vanish in the $r \rightarrow +\infty$ limit, yielding a more intricate expression for large distances. In fact, the Misner–Sharp mass for the quantum hairy corrected geometry yields

$$\lim_{r \rightarrow +\infty} m(r) = M \left(1 - \frac{\alpha}{2e^2} \right), \quad (79)$$

which is consistent with observing the coherent quantum GD hairy black hole very far from the quantum core, resembling the classical GD hairy limit [32]. For a tiny characteristic size of the quantum core, the Misner–Sharp mass reduces to

$$\lim_{R_s \rightarrow 0^+} m(r) = M \left(1 - \frac{\alpha}{2e^2} \right) - \frac{Q^2}{2r} - \alpha M e^{-r/G_N M}. \quad (80)$$

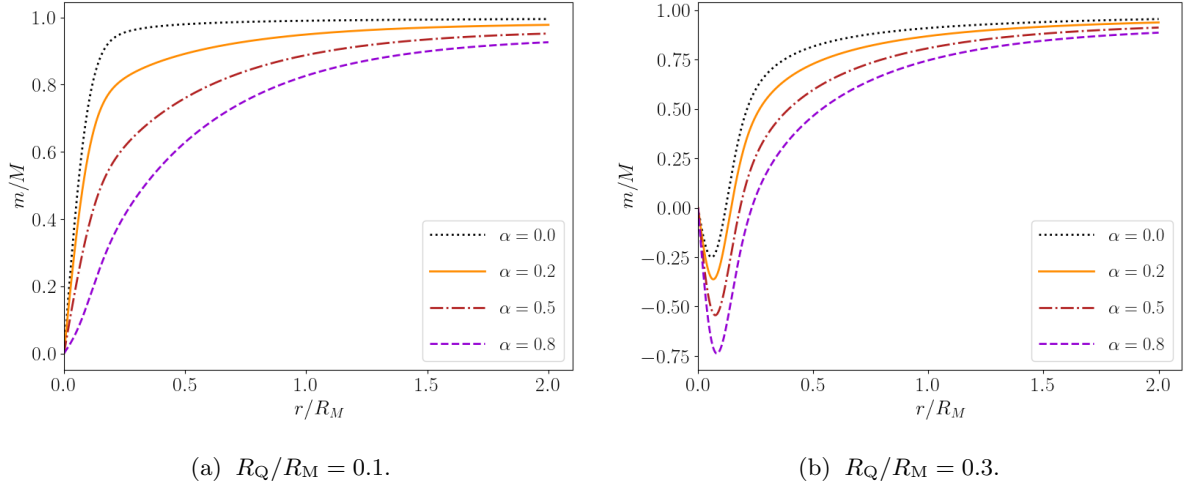


FIG. 5: Behavior of the normalized mass function $m(r)/M$ for fixed $R_s/R_M = 0.1$ and $R_Q/R_M = 0.1$ (left) and $R_Q/R_M = 0.3$ (right).

Fig. 5 shows the radial behavior of the normalized mass function $m(r)/M$ for different values of the hairy parameter α , with fixed $R_s/R_M = 0.1$ and two representative values of R_Q/R_M . For $R_Q/R_M = 0.1$ (left panel), the normalized mass function $m(r)/M$ increases monotonically from the origin and rapidly approaches its asymptotic value, with larger α delaying the saturation. On the other hand, for $R_Q/R_M = 0.3$ (right panel), the mass function develops a shallow negative region at small radii, whose depth increases as a function of α , while all curves still converge to the same asymptotic mass at large radial distance.

V. RESOLVING THE SINGULARITY AT THE ORIGIN

The metric function for the quantum-corrected GD hairy geometry $f(r) = 1 + 2V_{\text{GDH}}^q(r)$ is analytic. Therefore, it is possible to expand it around $r = 0$ through a power series as proposed in Ref. [78]:

$$f(r) = \sum_{n=0}^{\infty} f_n r^n, \quad (81)$$

where $f_n = \frac{f^{(n)}(0)}{n!}$. To check whether the quantum-corrected GD hairy geometry is regular around the origin, it is necessary to analyze the curvature invariants, which can be conveniently written in terms of the expansion coefficients of Eq. (81). These can be read up to $\mathcal{O}(r)$,

respectively, as [78]

$$\lim_{r \rightarrow 0^+} R = -\frac{2}{r^2}(f_0 - 1) - \frac{6}{r}f_1 - 12f_2, \quad (82a)$$

$$\begin{aligned} \lim_{r \rightarrow 0^+} R^\mu{}_\nu R^\nu{}_\mu &= \frac{2}{r^4}(f_0 - 1)^2 + \frac{8}{r^3}f_1(f_0 - 1) + \frac{2}{r^2} [6f_2(f_0 - 1) + 5f_1^2] \\ &\quad + \frac{4}{r} [4f_3(f_0 - 1) + 9f_1f_2] + 4 [5f_4(f_0 - 1) + 14f_1f_3 + 9f_2^2], \end{aligned} \quad (82b)$$

$$\begin{aligned} \lim_{r \rightarrow 0^+} R_{\mu\nu\rho\sigma} R^{\mu\nu\rho\sigma} &= \frac{4}{r^4}(f_0 - 1)^2 + \frac{8}{r^3}f_1(f_0 - 1) + \frac{8}{r^2} [f_2(f_0 - 1) + f_1^2] \\ &\quad + \frac{8}{r} [f_3(f_0 - 1) + 3f_1f_2] + 8 [f_4(f_0 - 1) + 4f_1f_3 + 3f_2^2]. \end{aligned} \quad (82c)$$

When $f_0 = 1$ and $f_1 = 0$, the three quantities (82a) – (82c) are finite:

$$R = -12f_2, \quad R^\mu{}_\nu R^\nu{}_\mu = 36f_2^2, \quad R_{\mu\nu\rho\sigma} R^{\mu\nu\rho\sigma} = 24f_2^2. \quad (83)$$

To check the geometry regularity, it is sufficient to calculate the f_0 , f_1 , and f_2 coefficients. Specializing to the quantum-corrected GD hairy metric function, given by $f(r)$ in Eq. (57), it follows that

$$f_0 = 1 + \frac{2}{R_s} \left(\frac{R_Q^2}{R_s} - \frac{R_M}{\sqrt{\pi}} \right) + \frac{2\alpha G_N \ell}{\sqrt{\pi} R_s} + 2\alpha \left[\frac{R_M}{\sqrt{\pi} R_s} - \operatorname{erfc} \left(\frac{R_s}{R_M} \right) e^{R_s^2/R_M^2} \right], \quad (84a)$$

$$f_1 = 0, \quad (84b)$$

$$f_2 = -\frac{4}{3R_s^3} \left(\frac{R_Q^2}{R_s} - \frac{R_M}{2\sqrt{\pi}} \right) - \frac{2\alpha G_N \ell}{3\sqrt{\pi} R_s^3} + \frac{2\alpha}{3} \left[\frac{2}{\sqrt{\pi} R_M R_s} - \frac{R_M}{\sqrt{\pi} R_s^3} - \frac{2}{R_M^2} \operatorname{erfc} \left(\frac{R_s}{R_M} \right) e^{R_s^2/R_M^2} \right]. \quad (84c)$$

Hence, two possible scenarios can be read off, depending on whether $f_0 = 1$ or $f_0 \neq 1$. If the first condition is satisfied, a regular configuration at $r = 0$ sets in, corresponding to a single, doubly-degenerate horizon.

Replacing the condition $f_0 = 1$ in Eq. (84a) and manipulating it, while using the extremal condition for the hair charge ℓ given in Eq. (28), we end up with the following equation:

$$\frac{R_Q^2}{R_M^2} = \frac{R_s}{\sqrt{\pi} R_M} - \frac{\alpha R_s}{\sqrt{\pi} R_M} \left(1 + \frac{1}{2e^2} \right) + \alpha \frac{R_s^2}{R_M^2} e^{R_s^2/R_M^2} \operatorname{erfc} \left(\frac{R_s}{R_M} \right). \quad (85)$$

Eq. (85) dictates which combination of values of R_Q/R_M and R_s/R_M yields a regular geometry to the coherent quantum GD hairy black hole. The small R_s/R_M limit yields

$$\frac{R_s}{R_M} = \frac{\sqrt{\pi}(R_Q^2/R_M^2 - \alpha)}{1 - 3\alpha - 1/2e^2}. \quad (86)$$

Therefore, for $R_s/R_M \ll 1$, it is possible to find values of R_s that make the geometry of the quantum GD hairy black hole to be regular at $r = 0$, for certain values of R_Q , R_M and α .

In a more general approach, we can solve Eq. (85) numerically for fixed values of α , and find a set of solutions for R_Q/R_M in terms of R_s/R_M . This can be visualized in Fig. 6.

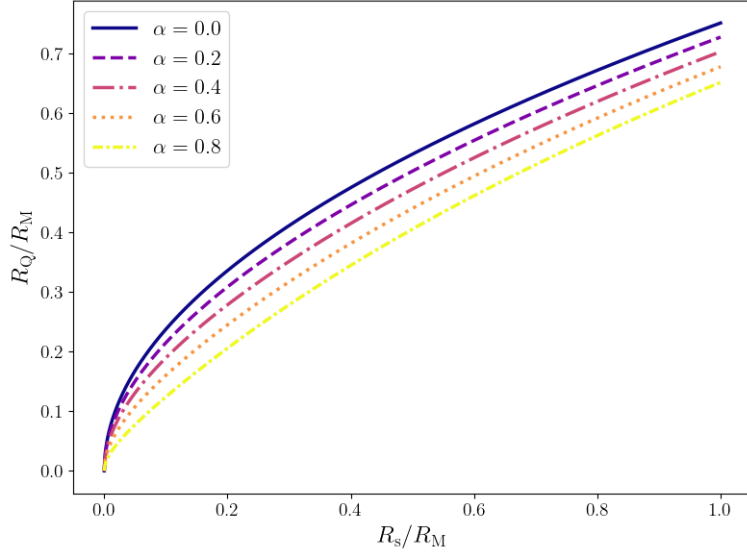


FIG. 6: Values of R_Q/R_M in terms of R_s/R_M that provide a regular geometry at the origin.

Fig. 6 illustrates the relation between the normalized parameters R_Q/R_M and R_s/R_M for different values of the hairy parameter α . In all cases, R_Q/R_M increases monotonically with R_s/R_M , defining a well-behaved parameter space for the solutions. Increasing α shifts the curves downward, indicating that stronger GD hairy effects reduce the allowed charge scale R_Q/R_M for a fixed stellar radius R_s/R_M .

On the other hand, if the case $f_0 \neq 1$ is considered, Eq. (85) does not hold anymore, and the quantum-corrected GD hairy geometry contains an integrable singularity at $r = 0$. As pointed out in Ref. [78], this emulates the case for the coherent quantum RN geometry, and even though the curvature invariants diverge, the integrable singularity is weaker than in the classical RN geometry [90]. The integrability of this singularity is due to the nature of the energy density function $\rho(r)$ (61) of the coherent quantum GD hairy geometry. Even though $\rho(r)$ is not regular at $r = 0$, as it can be seen clearly in Fig. 4, it yields a finite Misner–Sharp mass (77), which can also be seen in Fig. 5. The fact that the mass function vanishes at $r = 0$ can be explained by the finiteness nature of the potential V_{GDH}^q due to the quantum corrections of the coherent-state approach [90, 91].

VI. STRONG-FIELD PHOTON DYNAMICS AND OBSERVATIONAL SIGNATURES OF COHERENT QUANTUM GD HAIRY BLACK HOLES

The coherent quantum GD hairy black hole geometry significantly modifies the RN geometry. As a consequence, the existence of a quantum core and corrections due to the hairy parameter in the strong-curvature regime produce observable effects, allowing observational tests to constrain

the scale of modifications to GR.

In this section, we study the dynamical properties of both massive and massless particles in the geometry associated with coherent quantum GD hairy black holes and investigate how the hairy parameter affects observational properties beyond the classical RN geometry. Ref. [78] investigated how a purely coherent quantum RN black hole geometry affects observational properties of photons. This geometry is a particular case of coherent quantum GD hairy black holes for $\alpha = 0$ and $\ell = 0$. Ref. [80] considered a similar approach for a quantum Schwarzschild-like geometry and analyzed the dynamics of both massive and massless particles.

The standard approach to investigating geodesics is followed, considering the motion of point-like particles on the equatorial plane (corresponding to the azimuthal angle $\theta = \pi/2$) without loss of generality, due to the rotational isometry. The two Killing vectors corresponding to two constants of motion for particles on geodesics are the particle energy and its angular momentum, both quantities measured per unit mass, respectively given by [92]

$$E = f(r)\dot{t} \quad (87a)$$

$$L = r^2\dot{\phi}. \quad (87b)$$

Then, the geodesic equation reads:

$$\dot{r}^2 = E^2 - V_{\text{EFF}}(r), \quad (88)$$

where

$$V_{\text{EFF}} = f(r) \left(\frac{L^2}{r^2} - \mu \right), \quad (89)$$

with μ being the norm of the tangent vector to the geodesic, taking $\mu = -1, 0, 1$ whether the geodesic is timelike, null, or spacelike, respectively, and the dot sign denoting the derivative with respect to the affine parameter along the geodesic. Throughout this section, we will address the dynamics of photons in the spacetime defined by the coherent quantum GD hairy black hole metric, probing for observable astrophysical properties.

Since photons are massless particles, the geodesics are null. In this case, one can consider $\mu = 0$ in Eq. (89). A particularly relevant quantity to obtain is the photon rings R_γ . They can be derived through the condition $V'_{\text{EFF}}(R_\gamma) = 0$, which implies

$$R_\gamma f'(R_\gamma) - 2f(R_\gamma) = 0. \quad (90)$$

We can split Eq. (90) into two parts. The first one consists of the quantum contribution $f^q(r)$ (58) of $f(r)$ whose solution was found in Ref. [78], whereas the second one comprises the hairy

part $f^H(r)$ (59). It implies that Eq. (90) can be written as

$$[R_\gamma f'^q(R_\gamma) - 2f^q(R_\gamma)] + [R_\gamma f'^H(R_\gamma) - 2f^H(R_\gamma)] = 0. \quad (91)$$

The quantum part yields the following equation for R_γ :

$$1 - \frac{R_Q^2}{R_s^2} + \frac{R_M}{\sqrt{\pi}R_s} \exp\left(-\frac{R_\gamma}{R_s}\right) + \frac{R_Q^2(3R_s^2 + 2R_\gamma^2)}{R_\gamma R_s^3} F\left(\frac{R_\gamma}{R_s}\right) - \frac{3R_M}{2R_\gamma} \operatorname{erf}\left(\frac{R_\gamma}{R_s}\right) = 0. \quad (92)$$

The hairy component of the metric (57) yields the following photon ring equation, already imposing the lower bound condition (28) $G_N \ell = R_M/2e^2$:

$$\begin{aligned} & -\frac{3\alpha R_M}{2e^2 R_\gamma} \operatorname{erf}\left(\frac{R_\gamma}{R_s}\right) + \frac{2\alpha R_M}{\sqrt{\pi}R_s} \left(1 + \frac{1}{2e^2}\right) \exp\left(-\frac{R_\gamma}{R_s}\right) + \\ & + \alpha \operatorname{erfc}\left(\frac{R_s}{R_M} + \frac{R_\gamma}{R_s}\right) \exp\left(\frac{R_s^2}{R_M^2} + \frac{2R_\gamma}{R_M}\right) \left(\frac{3R_M}{2R_\gamma} - 1\right) - \\ & - \alpha \operatorname{erfc}\left(\frac{R_s}{R_M} - \frac{R_\gamma}{R_s}\right) \exp\left(\frac{R_s^2}{R_M^2} - \frac{2R_\gamma}{R_M}\right) \left(\frac{3R_M}{2R_\gamma} + 1\right) = 0. \quad (93) \end{aligned}$$

The photon ring equation for the coherent quantum GD hairy black hole model is given by a sum of Eqs. (92) and (93). It can only be solved through numerical methods, and the curves representing R_γ/R_M in terms of R_s/R_M are displayed in the plots in Fig. 7.

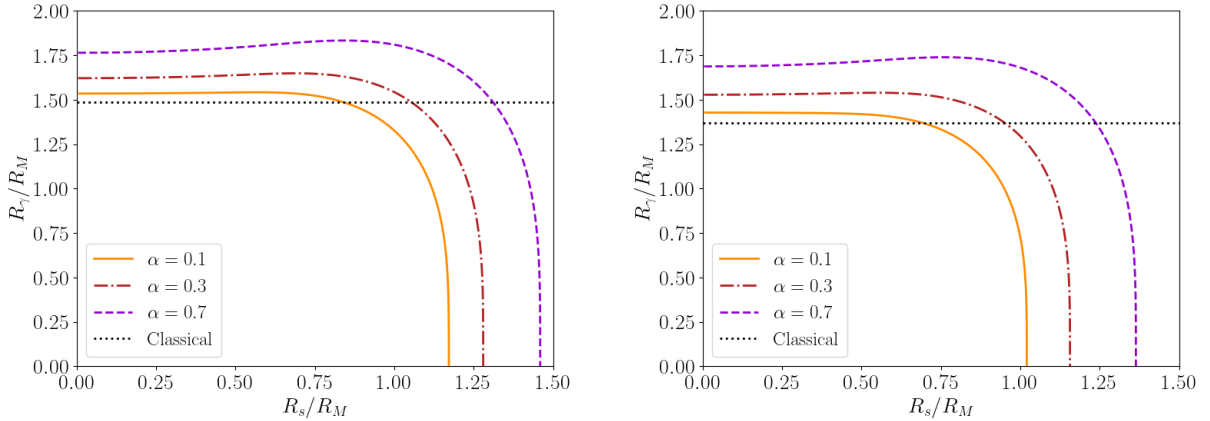


FIG. 7: Photon radius R_γ in units of R_M as a function of R_s/R_M for different values of the hairy parameter α . In the left panel, we set $R_Q/R_M = 0.1$ and in the right panel, we set $R_Q/R_M = 0.3$. The classical value for the photon radius is plotted as a dashed black line.

Fig. 7 shows the photon radius R_γ (in units of R_M) as a function of R_s/R_M for different values of the hairy parameter α , with $R_Q/R_M = 0.1$ (left panel) and $R_Q/R_M = 0.3$ (right panel). For each fixed value of α , the photon ring becomes slightly smaller as the ratio R_Q/R_M increases, while for fixed R_Q/R_M the photon radius increases with α , indicating the photon ring increases due to GD hair. At small and intermediate values of R_s/R_M , increasing α leads to

photon radii larger than the classical (quantum RN) value and extends the admissible range of R_s/R_M before the disappearance of circular photon orbits. However, for each fixed α there exists a critical regime in which the photon ring becomes smaller than that of the quantum RN black hole. In the weak-hair limit, all curves approach the classical photon radius, ensuring consistency with the standard case.

Once the photon radius is determined, it is possible to find the critical impact parameter, defined as

$$b_c = \frac{R_\gamma}{\sqrt{f(R_\gamma)}}. \quad (94)$$

Eq. (94) corresponds to the minimal impact parameter value $b = L/E$ below which the photon falls into the black hole. Since we have determined the photon radius R_γ numerically, the critical impact parameter is obtained similarly. Fig. 8 shows the behavior of b_c/R_M with respect to R_s/R_M .

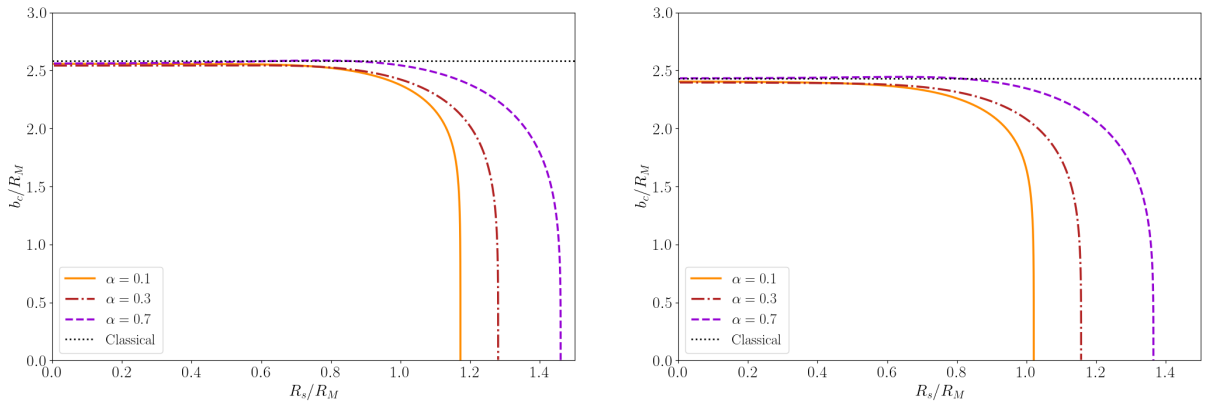


FIG. 8: Critical impact parameter b_c in units of R_M with respect to R_s/R_M for different values of the hairy parameter α . In the left panel, we set $R_Q/R_M = 0.1$ and in the right panel, we set $R_Q/R_M = 0.3$. In both plots, the classical photon ring is shown.

Fig. 8 shows the critical impact parameter b_c (in units of R_M) as a function of R_s/R_M for different values of the hairy parameter α , with $R_Q/R_M = 0.1$ (left panel) and $R_Q/R_M = 0.3$ (right panel). For fixed R_Q/R_M , increasing α enhances the critical impact parameter and extends the admissible range of R_s/R_M before the loss of unstable photon orbits. In the weak-hair regime, all curves approach the classical value, confirming consistency with the standard photon sphere behavior.

Another important observable variable is the gravitational lensing of light rays caused by the strong gravitational fields of black holes. Since the angular momentum is given by Eq. (87b), the geodesics of photons can be used to quantify the angular deflection of light in the coherent

quantum GD hairy black hole geometry, reading

$$\dot{\phi} = \pm \frac{\dot{r}}{r \sqrt{\frac{r^2}{b^2} - f(r)}}. \quad (95)$$

When $\dot{r} = 0$, the orbit presents a turning point at radius $r = r_0$. Imposing this position in Eq. (88), and using Eq. (87b), it is possible to determine that the impact parameter b can be written in terms of the turning point r_0 as

$$b = \frac{r_0}{\sqrt{f(r_0)}}. \quad (96)$$

To compute the angle variation of light $\Delta\phi$ due to the presence of the quantum-corrected GD hairy black hole, we must integrate Eq. (95), assuming that the light ray comes from infinity, reaches the turning point r_0 , and drifts off toward infinity in space. This yields:

$$\Delta\phi = 2 \int_{r_0}^{\infty} \frac{dr}{r \sqrt{\frac{r^2}{b^2} - f(r)}}. \quad (97)$$

The integral in Eq. (97) is computed numerically due to the high complexity of the metric function. The results are shown in Fig. 9, where the light deflection angle $\Delta\phi_d = \Delta\phi - \pi$ is plotted in terms of the normalized impact parameter b/R_M , with the influence of the hairy parameter α .

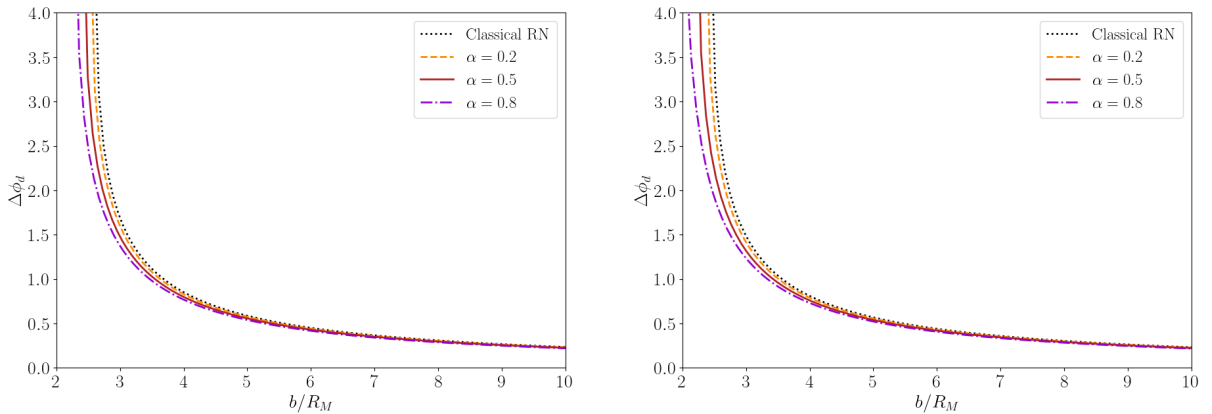


FIG. 9: Deflection angle $\Delta\phi_d = \Delta\phi - \pi$ of light due to the coherent quantum GD hairy black hole, in terms of the normalized impact parameter. In both plots, we used $R_s/R_M = 0.1$. In the left panel we set $R_Q/R_M = 0.1$, and in the right panel we set $R_Q/R_M = 0.3$.

Fig. 9 shows the light deflection angle as a function of the normalized impact parameter b/R_M for the coherent quantum GD hairy black hole, compared with the classical RN case. For fixed $R_s/R_M = 0.1$, increasing the hairy parameter α slightly reduces the deflection angle at small impact parameters, while all curves sharply converge at large b/R_M . The left and right

panels indicate that a larger charge increases the deviation from the classical RN behavior in the strong-lensing regime.

The observational properties studied here reveal that the GD hair charge causes relevant deviations from both the purely coherent quantum black hole model of [78] and the classical RN black hole. This implies that astrophysical observations may be used to test the coherent quantum GD hairy black hole model.

VII. CONCLUSIONS

In this work, we have constructed and analyzed a coherent quantum extension of the GD hairy black hole within the coherent-state framework of quantum black holes. The associated classical gravitational potential is interpreted as the expectation value of a canonically normalized scalar operator evaluated on a suitable coherent state, and UV divergences are regularized by a Gaussian smearing characterized by a fundamental length scale R_s . Applying this prescription to the GD hairy black hole yields a geometry that is asymptotically classical while developing a finite quantum core at short distances. The Gaussian regulator suppresses high-momentum modes in the Fourier–Bessel decomposition, eliminating the characteristic r^{-1} and r^{-2} singularities. As a result, the coherent quantum GD hairy metric function becomes analytic at the origin, with all curvature invariants remaining finite under suitable parameter conditions.

The classical GD hairy potential decomposes into an RN term and a Yukawa-like contribution controlled by the hair parameter α and the scale ℓ . After Gaussian regularization, both the electromagnetic and hairy sectors are finite at the origin. The resulting coherent quantum GD hairy spacetime smoothly interpolates between an asymptotically flat exterior and a nonsingular quantum core, preserving the large-distance behavior while resolving the central singularity. From the effective Einstein equations, the corresponding stress-energy tensor can be interpreted as an anisotropic quantum fluid. The energy density and pressures remain finite at the center, with a vacuum-like equation of state analogous to a de Sitter core. The difference between tangential and radial pressures reflects the intrinsic anisotropy induced by quantum smearing and hair contributions.

We also computed the Misner–Sharp mass function and showed that, while the quantum RN sector asymptotically reproduces the ADM mass M , the hairy corrections renormalize the total mass at infinity. For small values of R_s , the mass function reduces to the classical GD hairy expression with additional Yukawa-type corrections. The horizon structure of the coherent quantum GD hairy solution was investigated numerically. Depending on the values of (R_M, R_Q, R_s, α) , the coherent quantum GD hairy spacetime can exhibit two horizons, a

degenerate (extremal) configuration, or no horizon at all. The competition between charge, mass, quantum core size, and hair amplitude determines whether a black hole or a horizonless compact object forms. In particular, we derived the condition for regularity at the origin and identified parameter regions where the geometry is nonsingular.

Finally, we analyzed null geodesics in the quantum-corrected GD hairy background. The photon ring radius, critical impact parameter, and light deflection were computed numerically. Both the quantum core scale R_s and the hair parameter α produce measurable deviations from the classical and quantum RN cases, in the strong-field regime. These modifications leave imprints on black hole shadows and gravitational lensing, providing potential phenomenological settings to constrain the scale of quantum corrections and the presence of hair. The coherent quantum GD hairy black hole setup provides a self-consistent framework in which UV regularization, singularity resolution, modified horizon structure, and potentially observable strong-field signatures arise from a quantum description. The Gaussian smearing scale R_s governs the transition between classical geometry and a regular quantum core, while the hair parameter α controls deviations from the purely quantum-corrected RN case. Our results support the interpretation of GD hairy black holes as macroscopic quantum states whose classical singularities are softened, while admitting phenomenologically relevant hair.

Acknowledgements: HN is financed by the Coordination for the Improvement of Higher Education Personnel - Brazil (CAPES) - Finance Code 001. RdR is supported by The São Paulo Research Foundation (FAPESP) (Grants No. 2025/23004-9, No. 2021/01089-1, and No. 2024/05676-7) and the National Council for Scientific and Technological Development (CNPq) (Grants No. 303742/2023-2 and No. 401567/2023-0).

-
- [1] B. P. Abbott et al. (LIGO Scientific, Virgo), *Phys. Rev. D* **100**, 104036 (2019), 1903.04467.
 - [2] J. Ovalle, *Phys. Rev. D* **95**, 104019 (2017), 1704.05899.
 - [3] J. Ovalle, *Phys. Lett. B* **788**, 213 (2019), 1812.03000.
 - [4] Z. Yousaf, K. Bamba, B. Almutairi, S. Khan, and M. Z. Bhatti, *Class. Quant. Grav.* **41**, 175001 (2024), 2407.10451.
 - [5] E. Contreras, J. Ovalle, and R. Casadio, *Phys. Rev. D* **103**, 044020 (2021), 2101.08569.
 - [6] P. Leon and C. Las Heras, *Eur. Phys. J. C* **83**, 260 (2023).
 - [7] A. Ramos, C. Arias, E. Fuenmayor, and E. Contreras, *Eur. Phys. J. C* **81**, 203 (2021), 2103.05039.
 - [8] M. Sharif and T. Naseer, *Phys. Dark Univ.* **42**, 101324 (2023), 2310.00872.
 - [9] E. Morales and F. Tello-Ortiz, *Eur. Phys. J.* **C78**, 841 (2018), 1808.01699.
 - [10] G. Panotopoulos and A. Rincón, *Eur. Phys. J.* **C78**, 851 (2018), 1810.08830.
 - [11] K. N. Singh, S. K. Maurya, M. K. Jasim, and F. Rahaman, *Eur. Phys. J. C* **79**, 851 (2019).

- [12] L. Gavassino and J. Noronha, *Phys. Rev. D* **109**, 096040 (2024), 2305.04119.
- [13] D. Berkimbayev, *Eur. Phys. J. C* **86**, 55 (2026), 2511.18485.
- [14] C. L. Heras and P. Leon, *Fortsch. Phys.* **66**, 1800036 (2018), 1804.06874.
- [15] V. A. Torres-Sánchez and E. Contreras, *Eur. Phys. J.* **C79**, 829 (2019), 1908.08194.
- [16] S. Hensh and Z. Stuchlík, *Eur. Phys. J. C* **79**, 834 (2019), 1906.08368.
- [17] S. K. Maurya, G. Mustafa, S. Ray, B. Dayanandan, A. Aziz, and A. Errehymy, *Phys. Dark Univ.* **42**, 101284 (2023).
- [18] N. Iqbal, M. Amir, M. Alshammari, W. W. Mohammed, and M. Ilyas, *Eur. Phys. J. C* **85**, 428 (2025).
- [19] F. Tello-Ortiz, P. Bargueño, A. Alvarez, and E. Contreras, *Fortsch. Phys.* **71**, 2200170 (2023).
- [20] M. Khatoun, I. Mahmood, H. Sohail, A. Ditta, H. O. Elansary, X.-Y. Liu, A. Ashraf, and S. Mannanova, *Eur. Phys. J. C* **85**, 1102 (2025).
- [21] M. Zubair, H. Sohail, S. Waheed, A. Ilyas, and I. Mahmood, *Chin. Phys. C* **50** (2026).
- [22] R. da Rocha, *Phys. Rev. D* **95**, 124017 (2017), 1701.00761.
- [23] P. Meert and R. da Rocha, *Nucl. Phys. B* **967**, 115420 (2021), 2006.02564.
- [24] R. Casadio, P. Nicolini, and R. da Rocha, *Class. Quant. Grav.* **35**, 185001 (2018), 1709.09704.
- [25] R. da Rocha and J. M. Hoff da Silva, *Phys. Rev. D* **85**, 046009 (2012), 1202.1256.
- [26] R. da Rocha and A. A. Tomaz, *Eur. Phys. J. C* **80**, 857 (2020), 2005.02980.
- [27] R. T. Cavalcanti, A. G. da Silva, and R. da Rocha, *Class. Quant. Grav.* **33**, 215007 (2016), 1605.01271.
- [28] X.-J. Wang, Y. Meng, X.-M. Kuang, and K. Liao, *Phys. Rev. D* **112**, 124016 (2025), 2508.02355.
- [29] Y. Liang, X. Lyu, and J. Tao, *Commun. Theor. Phys.* **76**, 085402 (2024).
- [30] L. Gabbanelli, A. Rincón, and C. Rubio, *Eur. Phys. J. C* **78**, 370 (2018), 1802.08000.
- [31] Z. Li, *Phys. Lett. B* **841**, 137902 (2023), 2212.08112.
- [32] J. Ovalle, R. Casadio, E. Contreras, and A. Sotomayor, *Phys. Dark Univ.* **31**, 100744 (2021), 2006.06735.
- [33] A. Rincón, L. Gabbanelli, E. Contreras, and F. Tello-Ortiz, *Eur. Phys. J. C* **79**, 873 (2019), 1909.00500.
- [34] R. Avalos, P. Bargueño, and E. Contreras, *Fortsch. Phys.* **2023**, 2200171 (2023), 2303.04119.
- [35] A. M. Albalahi, Z. Yousaf, A. Ali, and S. Khan, *Eur. Phys. J. C* **84**, 9 (2024).
- [36] M. Sharif, T. Naseer, and H. Shadab, *Chin. J. Phys.* **97**, 1386 (2025).
- [37] J. Andrade, D. Santana, T. Naseer, E. P. Valdiviezod, and D. T. C. Ortiz, *Eur. Phys. J. C* **85**, 1174 (2025).
- [38] H. L. Prihadi, D. Dwiputra, F. Khairunnisa, and F. P. Zen, *Eur. Phys. J. C* **85**, 946 (2025), 2501.01680.
- [39] S. K. Maurya, M. K. Jasim, A. Errehymy, K. Boshkayev, G. Mustafa, and B. Dayanandan, *Phys. Dark Univ.* **46**, 101665 (2024).
- [40] O. A. Almatroud, M. Rizwan, M. Alshammari, M. Z. Bhatti, S. Alshammari, and Z. Yousaf, *Eur. Phys. J. C* **85**, 1285 (2025).
- [41] S. K. Maurya, F. Al Khayari, A. Ashraf, M. K. Jasim, S. T. T., and P. Channuie, *Chin. J. Phys.* **96**, 621 (2025).
- [42] C.-M. Zhang, M. Zhang, and D.-C. Zou, *Chin. Phys. C* **47**, 015106 (2023), 2208.06830.
- [43] J. Lin, M. Bravo-Gaete, and X. Zhang, *Phys. Rev. D* **109**, 104039 (2024), 2401.02045.
- [44] V. F. Guimarães, R. T. Cavalcanti, and R. da Rocha, *Class. Quant. Grav.* **42**, 175011 (2025), 2506.20044.
- [45] R. T. Cavalcanti, R. C. de Paiva, and R. da Rocha, *Eur. Phys. J. Plus* **137**, 1185 (2022), 2203.08740.
- [46] G. P. Ribeiro, R. B. Magalhães, and L. C. B. Crispino, *Phys. Rev. D* **112**, 124082 (2025), 2512.04377.
- [47] Y. Yang, D. Liu, A. Övgün, Z.-W. Long, and Z. Xu, *Phys. Rev. D* **107**, 064042 (2023), 2203.11551.
- [48] R. Avalos and E. Contreras, *Eur. Phys. J. C* **83**, 155 (2023), 2302.09148.

- [49] A. Al-Badawi, S. K. Jha, and A. Rahaman, *Eur. Phys. J. C* **84**, 145 (2024).
- [50] F. Tello-Ortiz, R. Avalos, Y. Gómez-Leyton, and E. Contreras, *Phys. Dark Univ.* **46**, 101547 (2024).
- [51] A. Ditta, F. Javed, S. K. Maurya, G. Mustafa, and F. Atamurotov, *Phys. Dark Univ.* **42**, 101345 (2023).
- [52] N. Mansour, T. Toghrayi, A. El Boukili, A. Benami, A. K. Daoudia, and M. B. Sedra, *Int. J. Mod. Phys. A* **39**, 2450151 (2024).
- [53] S. Mahapatra and I. Banerjee, *Phys. Dark Univ.* **39**, 101172 (2023), 2208.05796.
- [54] M. Misyura, A. Rincon, and V. Vertogradov, *Phys. Dark Univ.* **46**, 101717 (2024), 2405.05370.
- [55] D. Astefanesei, R. Ballesteros, P. Cabrera, G. Casanova, and R. Rojas, *Phys. Rev. D* **110**, 024045 (2024), 2404.15566.
- [56] H. Rehman and G. Abbas, *Chin. Phys. C* **47**, 125106 (2023).
- [57] R. Casadio, A. Giusti, I. Kuntz, and G. Neri, *Phys. Rev. D* **103**, 064001 (2021), 2101.12471.
- [58] R. Casadio, A. Giugno, A. Giusti, and M. Lenzi, *Phys. Rev. D* **96**, 044010 (2017), 1702.05918.
- [59] R. Casadio, *Int. J. Mod. Phys. D* **31**, 2250128 (2022), 2103.00183.
- [60] W. Mück, *Eur. Phys. J. C* **76**, 374 (2016), 1606.01790.
- [61] R. Casadio, A. Giugno, and A. Orlandi, *Phys. Rev. D* **91**, 124069 (2015), 1504.05356.
- [62] A. Giusti, *Int. J. Geom. Meth. Mod. Phys.* **16**, 1930001 (2019).
- [63] R. Casadio, A. Giugno, and A. Giusti, *Phys. Lett. B* **763**, 337 (2016), 1606.04744.
- [64] G. Dvali and C. Gomez, *Fortsch. Phys.* **61**, 742 (2013), 1112.3359.
- [65] G. Dvali and C. Gomez, *Phys. Lett. B* **719**, 419 (2013), 1203.6575.
- [66] D. Flassig, A. Pritzel, and N. Wintergerst, *Phys. Rev. D* **87**, 084007 (2013), 1212.3344.
- [67] S. Hofmann and T. Rug, *Nucl. Phys. B* **902**, 302 (2016), 1403.3224.
- [68] R. Casadio and A. Orlandi, *JHEP* **08**, 025 (2013), 1302.7138.
- [69] R. Casadio, R. T. Cavalcanti, A. Giugno, and J. Mureika, *Phys. Lett. B* **760**, 36 (2016), 1509.09317.
- [70] R. Casadio, A. Giusti, and J. Ovalle, *Phys. Rev. D* **105**, 124026 (2022), 2203.03252.
- [71] M. Cadoni, R. Casadio, A. Giusti, and M. Tuveri, *Phys. Rev. D* **97**, 044047 (2018), 1801.10374.
- [72] R. Casadio, *Ukr. J. Phys.* **69**, 466 (2024).
- [73] W. Feng, R. da Rocha, and R. Casadio, *Eur. Phys. J. C* **84**, 586 (2024), 2401.14540.
- [74] X. Calmet, R. Casadio, S. D. H. Hsu, and F. Kuipers, *Phys. Rev. D* **108**, 086012 (2023), 2305.09466.
- [75] R. Casadio, R. da Rocha, A. Giusti, and P. Meert, *Phys. Rev. D* **110**, 104067 (2024), 2407.04146.
- [76] R. Casadio, R. da Rocha, A. Giusti, and P. Meert, *Phys. Lett. B* **849**, 138466 (2024), 2310.07505.
- [77] W. Feng, A. Giusti, and R. Casadio, *Eur. Phys. J. Plus* **140**, 145 (2025), 2408.17091.
- [78] T. Antonelli, M. Sebastianutti, and A. Giusti, *Eur. Phys. J. C* **85**, 1219 (2025), 2506.02231.
- [79] P. Meert, A. Giusti, and R. Casadio, *Phys. Lett. B* **867**, 139613 (2025), 2504.02786.
- [80] A. Urmanov, H. Chakrabarty, and D. Malafarina, *Phys. Rev. D* **110**, 044030 (2024), 2406.04813.
- [81] D. J. Cirilo-Lombardo and N. G. Sanchez, *Phys. Rev. D* **108**, 126001 (2023), 2312.06628.
- [82] M. Zubair, H. Azmat, and H. Jameel, *Eur. Phys. J. C* **83**, 905 (2023).
- [83] K. Bamba, M. Z. Bhatti, Z. Yousaf, and Z. Shoukat, *Eur. Phys. J. C* **83**, 1033 (2023), 2307.10399.
- [84] M. Estrada, *Eur. Phys. J.* **C79**, 918 (2019), 1905.12129.
- [85] M. Sharif and A. Majid, *Chin. J. Phys.* **68**, 406 (2020).
- [86] S. Mahapatra, S. Priyadarshinee, G. N. Reddy, and B. Shukla, *Phys. Rev. D* **102**, 024042 (2020), 2004.00921.
- [87] S. Pradhan, S. K. Maurya, A. Errehymy, G. Mustafa, and P. K. Sahoo, *Chin. Phys.* **49**, 105110 (2025).
- [88] S. Priyadarshinee, S. Mahapatra, and I. Banerjee, *Phys. Rev. D* **104**, 084023 (2021), 2108.02514.

- [89] T. Naseer, M. Sharif, and S. Yaqoob, *Nucl. Phys. B* **1020**, 117180 (2025).
- [90] V. N. Lukash and V. N. Stokov, *International Journal of Modern Physics A* **28**, 13 (2013), 1301.5544.
- [91] J. Arrechea, S. Liberati, H. Neshat, and V. Vellucci, *Phys. Rev. D* **112**, 29 (2025), 2504.17863.
- [92] C. G. Boehmer, G. De Risi, T. Harko, and F. S. N. Lobo, *Class. Quant. Grav.* **27**, 185013 (2010), 0910.3800.